Accepted Manuscript

Influence of synthesis parameters on the physicochemical and electrochemical properties of $LiFePO_4$ for Li-ion battery

Swapnil J. Rajoba, Lata D. Jadhav, Ramchandra S. Kalubarme, Sanket N. Yadav

PII: S0925-8388(18)33583-7

DOI: 10.1016/j.jallcom.2018.09.325

Reference: JALCOM 47744

To appear in: *Journal of Alloys and Compounds*

Received Date: 18 July 2018

Revised Date: 24 September 2018

Accepted Date: 25 September 2018

Please cite this article as: S.J. Rajoba, L.D. Jadhav, R.S. Kalubarme, S.N. Yadav, Influence of synthesis parameters on the physicochemical and electrochemical properties of $LiFePO_4$ for Li-ion battery, *Journal of Alloys and Compounds* (2018), doi: https://doi.org/10.1016/j.jallcom.2018.09.325.

Influence of synthesis parameters on the physicochemical and electrochemical properties of $LiFePO_4$ for Li-ion battery

Swapnil J. Rajoba[1], Lata D. Jadhav[1*], Ramchandra S. Kalubarme[2], Sanket N. Yadav[3]

[1]Electrochemical Energy Materials Laboratory, Department of Physics, Rajaram College. Kolhapur - 416 004, India

[2]Centre for Materials for Electronics Technology, Thrissur-680581, India

[3]School of Nano Science and Technology, Shivaji University, Kolhapur-416004, India

* Corresponding author: ldjadhav.phy@gmail.com

Abstracts:

$LiFePO_4$ (LFP) has been developed as a cathode for lithium ion batteries (LIBs) by solution combustion method. The present work includes effect of fuel, residual carbon and graphene oxide on the phase purity and electrochemical performance of combustion synthesized $LiFePO_4$. As revealed in XRD, single phase $LiFePO_4$ is obtained in glycine assisted combustion (G-LFP) and it delivers 97 mA.h/g discharge capacity, which is higher than urea assisted combustion (U-LFP). Further, the G-LFP was calcined for different lengths of time (4, 5 and 7 hrs). The amount of in-situ carbon is observed to decrease from 2.57 to 1.40 % and specific capacity increases from 97 (4 hr) to 106 mA.h/g (7 hr). The composites with 4 wt. % GO were formed and they show enhanced electrochemical performance. 5LFP/GO delivers discharge capacity of 164 mA.h/g at 0.1 C, which is 96 % of its theoretical capacity.

Keywords: Lithium iron phosphate; Solution combustion; Fuel; graphene oxide and electrochemical performance.

1. Introduction:

Lithium ion batteries (LIBs) are one of the most popular secondary batteries for portable electronic devices due to their high energy and power densities, long cycle life and a broad temperature range of operation **[1]**. The selection of active materials and electrolyte especially, cathode material, is very critical governing the energy and power densities. Frequently, oxide materials with layered $LiMO_2$ (M= Co, Ni, and Mn) **[2]**, spinel $LiMn_2O_4$ **[3]** and olivine $LiFePO_4$ **[4]** type structures are used as cathode for LIBs. Among these materials, $LiFePO_4$ (LFP) exhibits high theoretical capacity (~170 mAh/g) **[5]**. Moreover, it is stable, low cost and environmentally friendly material **[6]**. Nevertheless, due to its slow Li-ion diffusion rate (~10^{-14} cm^2/s) and poor electronic conductivity (~10^{-9} s/cm) **[7]**, it is difficult to achieve the theoretical capacity. The three routes to raise the observed capacity to

theoretical one include carbon coating, particle size reduction and metal ion doping. Many reports are found on decorating the LFP particles with highly conducting carbon like CNTs, reduced graphene oxide (r-GO) and graphene **[8]**. At the same, different techniques such as solid state **[9]**, co-precipitation **[10]**, hydrothermal **[11]**, sol-gel **[12]** and solution combustion synthesis (SCS) **[13]** have been used to obtain nano-sized LFP particles. The synthesis method should be simple, rapid, low cost and safe and SCS meets all these criteria. It requires short reaction time and easy to control metal ion doping and purity of obtained product **[14-15]**.

In SCS, metal nitrates or precursor react with fuel and oxides are formed. Fuel acts as a complexing agent as well as it serves as a fuel during auto-ignition **[16]**. The large number of gases, heat and light energy released during auto ignition affect the physical properties of the material, which can be controlled by altering either type or amount of fuel or both **[17]**. Few reports are found on the synthesis of LFP by SCS **[13, 18]** since single phase LFP is difficult to achieve due to transfer of Fe^{2+} to Fe^{3+} during combustion. The reducing atmosphere, for proper combination of fuel and its amount, can be generated to avoid the oxidation of Fe. B. Zhao et al **[19]** varied the amount of fuel and have found that single phase LFP could be obtained at fuel rich condition. The specific capacity was also found to vary from 20 to 100 mAh/g. In SCS, carbon coating is possible both by residual carbon and carbon additives. The capacity of former is ~ 106 mAh/g while that of later is ~164 mAh/g **[20]**.

The aim of the current article is to investigate effect of fuel on the physical and electrochemical properties of LFP. Two fuels urea (CH_4N_2O) and glycine ($C_2H_5NO_2$) with reducing powers +6 and +9, respectively are used. Further, glycine has high negative combustion heat (-3.24 Kcal/g) than urea (-2.98 Kcal/g), leading to different powder properties **[21]**. The composite LFP/GO has also been formed and studied. An excess residual carbon resists Li-ion diffusion and hence needs to be controlled by applying post-heat treatments. Therefore, electrochemical performance of powder calcined for different lengths of time has also been investigated.

2. Experimental:

$LiFePO_4$ powder was synthesized by solution combustion synthesis (SCS). Iron nitrate ($FeN_3O_9.9H_2O$, Alfa Aesar 98-101%), ammonium di hydrogen phosphate ($NH_4H_2PO_4$, Alfa Aesar 98%) and lithium nitrate ($LiNO_3$, Alfa Aesar 99%) were used as metal precursors. Glycine ($C_2H_5NO_2$, Himedia 99%) and urea (CH_4N_2O, Thomas baker 99%) were used as

fuel. The metal nitrates and a phosphate precursor were dissolved in the minimum amount of double distilled water and kept on hot plate for constant stirring and heating. Then fuel dissolved in water was added into the solution of metal nitrate precursor, it helped mixing metal nitrates at molecular level to make a homogeneous mixture. The stoichiometric oxidant to fuel ratio for glycine was 1:2 and for urea 1:3. The gel was formed by removal of excess water during the process of constant heating and stirring. This gel was kept in a pre heated furnace, it was decomposed and ash was formed. The powders were named G-LFP and U-LFP for glycine and urea respectively. After grinding and homogenation in agate mortar, the powders were calcined in the tube furnace. The G-LFP and U-LFP powders were calcined at 700 and 650°C, respectively with heating rate of 10 °C/min for 4 hr in inert atmosphere. The temperatures were as deduced from TG-DTA analysis **[22]**.The calcination was performed under the flow of nitrogen gas to prevent oxidation of LFP and formation of iron oxide. In our previous report, 11.57 weight (%) of residual carbon was observed **[20]**. To reduce their residual carbon, all the calcined powders were again heat treated for 4 hr in 3 % H_2 + 97 % Ar atmosphere. The graphene oxide (GO) was synthesized from graphite using modified Hummers method. The detailed synthesis of GO is explained elsewhere **[23]**.

The crystalline properties of calcined $LiFePO_4$ powders were carried out by using X-ray diffractometer (PHILIPS PW-3710) with Cu K_α as radiation source. Morphological properties were analyzed using scanning electron microscope (SEM, JEOL JSM-6360). The vibrational spectroscopic studies were carried out by Raman spectroscopy (Bruker AXE Analytical Instrument PVT. Germany). The specific surface area was calculated from N_2 adsorption desorption isotherms measured using a Quantachrome Instrument (Model -NOVA 1000E) using the Brunauer-Emmett-Teller (BET) equation. The carbon content in the calcined $LiFePO_4$ was determined by elemental organic analysis (FLASH EA 1112 series, Italy).

2.1 Electrode fabrication:

To prepare cathode material, $LiFePO_4$ was mixed in a carbon black and polyvinylidene fluoride (PVDF) with a weight ratio 70:20:10 in N-methyl-2- pyrrolidone (NMP). The resultant slurry was casted on aluminum foil by doctor blade method and dried at 120 °C for 12 hr. The dried films were punched into round plates with diameter 1.6 mm. Lithium metal foil and celgard 2400 membrane were used as a counter electrode and separator respectively, while $LiPF_6$ in ethylene carbonate, dimethyl carbonate and diethyl carbonate (1:1:1) was used as electrolyte. The coin type half cells were assembled in argon filed glove box. The electrochemical performance of cells such as galvanostatic charge

discharge and cyclic voltammetry were performed in the voltage range 2.5 to 4.3 V Vs Li using Biologic-108 battery cycler. The voltages mentioned henceforth were recorded with respect to Li foil.

3. Results and discussion:

3.1: Effect of fuels on powder properties and electrochemical performance:

Fig. 1 demonstrates XRD patterns of calcined G-LFP and U-LFP. Both patterns match well with JCPDS card no. 40-1499 of $LiFePO_4$. In addition, diffraction peaks at 24.4 and 33.26° corresponding to Fe_2O_3 as well as diffraction peak of $Li_3Fe_2(PO_4)_3$ at 27.43° are observed in the XRD pattern of U-LFP (Fig. 1b). Despite the powders were calcined in inert atmosphere, the U-LFP is not phase pure. Certainly, these secondary phases have formed during autoignition. On the contrary, G-LFP is a single phase. Glycine being a larger molecule than urea, it generates more gases, which limits the rise in temperature and avoids the formation of agglomeration **[24-25]**. Moreover, relatively more reducing atmosphere created during combustion prevents the formation of secondary phases like Fe_2O_3. But this leaves behind more carbon in the powder. The amount of residual carbon in the calcined powders was estimated using elemental organic analysis (CHNS) [supporting documents Fig. 1 and 2]. The percentage of residual carbon is 2.57 and 0.065, respectively in G-LFP and U-LFP.

Fig. 2 shows Raman spectra of G-LFP and U-LFP. Raman spectrum of G-LFP (Fig. 2a) shows three bands in the region 900 to 1100 cm^{-1}. The band at 1050 cm^{-1} is assigned to the symmetric P-O stretching vibration mode while other bands are assigned to the antisymmetric stretching mode of $(PO_4)^{3-}$ **[26]**. In addition, bands observed at 209, 278, 391 and 628 cm^{-1} are assigned to the olivine structure of $LiFePO_4$ **[27]**. Apart from vibration modes of the LFP phase, the presence of ferric component is observed in the U-LFP (Fig. 2b) at 445 and 579 cm^{-1} **[28]**.

Effect of fuel on the surface properties and pore size distribution are studied by using Brunnauer-Emmett-Teller (BET) analysis of adsorption isotherms and are shown in Fig. 3. Both G-LFP and U-LFP show type III isotherm. The measured surface area for G-LFP and U-LFP is 7.73 and 8.93 m^2/g, respectively. The different surface areas may be due to elimination of different amounts of carbon during calcination. In addition, Barrett-Joyner-Halenda (BJH) method was used to calculate pore size distribution. The average pore radius of 9 and 5 nm is observed for G-LFP and U-LFP.

The gases evolved during the combustion and the local temperature affect the morphology as clearly observed in SEM image (Fig. 4). Porous, uniform and very small grains are observed in G-LFP compared to U-LFP, obviously, because of large number of gases released during combustion as compared to U-LFP. In U-LFP the least number of gases are unable to remove heat energy causing particles to agglomerate.

3.1.2 Electrochemical performance:

The cyclic voltammetry curves of G-LFP and U-LFP for the first cycle in the voltage range 2.5 to 4.3 V at 0.1 mV/s are shown (Fig. 5). A single pair of redox peak is observed in G-LFP (Fig. 5a). It reveals the single electron mechanism and it acts as key role during reversibility of Li-ion insertion and de-insertion. On the other hand, two pairs of well-separated redox peaks are clearly observed for U-LFP (Fig. 5b), indicating two step Li-ion insertion and de-insertion mechanism because of the presence of electroactive secondary phases as detected in the XRD pattern. These broad peaks with almost double potential difference suggest slowed diffusion process due to capacitive effects. In addition, the observed peak intensity reveals that G-LFP is more conducting than U-LFP.

The charge discharge profiles of G-LFP and U-LFP at 0.1 C as a function of specific capacity are shown in the Fig. 6. The G-LFP and U-LFP deliver the specific capacity of 97 and 55 mA.h/g, respectively. In the charge discharge profile of U-LFP, two distinct plateaus are observed. The second plateau is due to the presence of an electroactive impurity. On the other hand, a single plateau is observed in G-LFP with minimum polarization and faster lithium ion diffusion. Thus the presence of secondary phase with Fe in +3 state restricts the capacity in U-LFP.

3.2 Effect of calcination time:

It is inferred from the aforementioned results that the phase purity as well as residual carbon content is governed by the fuel. Glycine gives single phase powder but with excess residual carbon, which can be minimized by applying calcination for longer lengths of time (> 4hour). Therefore, G-LFP powders were calcined for 5 and 7 hour at 700°C. The samples were named as 4LFP, 5LFP and 7LFP.

XRD patterns of 4 LFP, 5LFP, and 7 LFP are shown in Fig. 7. No major change in the crystal structure is detected as shown in Fig. 7. Only crystallanity is observed to enhance with increase in calcination time. It is 18 nm for 4LFP, 19 nm for 5LFP and 22 nm for 7LFP. In addition, intensity ratio of the highest intense plane (131) with (111) plane (I_{131}/I_{111}) is observed to increase with the calcination time. The CHNS analysis showed that [Supporting documents Fig. 1, 3 and 4] the carbon content is 1.78 % for 5LFP and 1.47 % for 7LFP. SEM

images (Fig. 8) reveal that grain size as well as porosity increase with the increase in length of calcination time. The observed average grain size is 0.25 μm for 4LFP, 0.34 μm for 5LFP and 0.39 μm for 7LFP (Fig. 5 in the supporting document).

3.2.1 Electrochemical performance:

The charge-discharge profiles of 4LFP, 5LFP and 7LFP are shown in Fig. 9 and the discharge capacity at 0.1 C is 97, 106 and 106 mA.h/g and the coulombic efficiency is 97, 96 and 94 %, respectively. In addition, charge-discharge profiles at various C rates from 0.1 to 2 C were recorded to investigate the effect of calcination time on the rate performance (Fig. 10). With increasing C rate, the discharge capacity is observed to decrease due to the rise of electrode polarization. At higher current, 5LFP is more stable than 4LFP and 7LFP. The capacity fading after 40 cycles in 4LFP, 5LFP and 7LFP is 95, 94 and 97 %. From these results, it is observed that proper amount of carbon is imperative for the optimum electrochemical performance of $LiFePO_4$.

3.3 Effect of graphene oxide:

Although, the powder with residual carbon has delivered the highest discharge capacity of 106 mA.h/g, it is too low than its theoretical capacity (170 mA.h./g). Obviously, it is due to low electronic as well as ionic conductivity. In our earlier article **[20]**, 4 wt. % of graphene oxide (GO) has been found to enhance the electrochemical performance of LFP. So composites of 5LFP and 7LFP with 4 wt. % of GO were formed, named as 5LFP/GO and 7LFP/GO, respectively.

3.3.1 Electrochemical performance:

The cyclic voltammetry profiles of 7LFP/GO and 5LFP/GO at 0.1 mV/s are shown in Fig. 11. As compared to 5LFP/GO, sharp redox peaks with improved current densities are observed in 7LFP/GO. However, the potential difference between cathodic and anodic peak is observed to increase in 7LFP/GO, due to the increase in polarization. In addition, 7LFP/GO has small tail at the lower potential side. It reveals the presence of minute electroactive impurity, not observed in XRD, which enhances the electronic conductivity of material but it restricts Li-ion diffusion.

The charge discharge profiles of 5LFP/GO and 7LFP/GO for charging up to 4.3V and discharging up to 2.5 V at the cycling rate of 0.1C are compared in Fig. 12. An improvement in the specific discharge capacity is observed after the addition of GO. The specific discharge capacity at 0.1 C for 5LFP/GO is 164 mA.h/g and for 7LFP/GO is 154 mA.h/g, higher than that of 4LFP, 5LFP and 7LFP. These results reveal that due to the higher Li-ion diffusion

5LFP/GO composite has higher specific discharge capacity. In view of all the results, 5LFP/GO is optimum composite.

4. Conclusion:

In summary, a single phase $LiFePO_4$ is obtained for glycine assisted combustion (G-LFP) while secondary phases are found in the urea assisted combustion (U-LFP). These respectively leads to single electron mechanism with discharge capacity of 97 mA.h/g and two step diffusion mechanism with discharge capacity of 55 mA.h/g. Further, the amount of residual carbon in the powder can be controlled by duration of post heat treatment. It is decreased from 2.57 (4 hr) to 1.40 % (7 hr). It enhances the crystallanity, grain size and porosity. However, almost equal discharge capacities are obtained for 5LFP and 7LFP. The composites 5LFP/GO and 7LFP/GO exhibit discharge capacities 164 and 154 mA.h/g respectively. Higher Li-ion diffusion and sufficient electronic conductivity makes 5LFP/GO an optimum composite.

5. Acknowledgement:

The authors are very much thankful to Board of Research in Nuclear Sciences (BRNS) for the financial assistance under project no. 37(2)/14/10/2015/BRNS.

6. References:

1 C. Gong , Z. Xue, S. Wen, Y. Ye, X. Xie, "Advanced carbon materials/olivine $LiFePO_4$ composites cathode for lithium ion batteries", J. Power Sources, **318** (2016) 93-112.

2 Xiaohui Li, Zhi Su, Yingbo Wang, Electrochemical properties of monoclinic and orthorhombic $LiMnO_2$ synthesized by a one-step hydrothermal method, J. Alloys Compd. **735** (2018) 2182-2189.

3 A. M. Hashem, A. E. Abdel-Ghany, H. M. Abuzeid, R. S. El-Tawil, S. Indris, H. Ehrenberg, A. Mauger, C. M. Julien, "EDTA as chelating agent for sol-gel synthesis of spinel $LiMn_2O_4$ cathode material for lithium batteries", J. Alloys Compd., 10.1016/j.jallcom.2017.12.153.

4 L. Bao, L. Lia, , Gang Xua, J. Wanga, R. Zhaoa , G. Shena , G. Hana, S. Zhou, "Olivine $LiFePO_4$ nano crystallites embedded in carbon-coating matrix for high power Li-ionbatteries", Electrochim. Acta, **222** (2016) 685-692.

5 M. Y. Cho, K. B. Kim, J. W. Lee, H. Kim, H. Kim, K. Kang, K. C. Roh, "Defect-free solvothermally assisted synthesis of micro spherical mesoporous $LiFePO_4$/C", RSC Adv. **3** (2013) 3421-3427.

6 A. Fedorkova, R. Orinakova, O. Cech, M. Sedlarikova, "New Composite Cathode Materials for Li/S Batteries: A Review", Int. J. Electrochem. Sci., **8** (2013) 10308 – 10319.

7 Z. Bi, X. Zhang, W. He, D. Min, W. Zhang, "Recent advances in $LiFePO_4$ nanoparticles with different morphology for high-performance lithium-ion batteries", RSC Adv.**3** (2013) 19744-19751.

8 J. P. Jegal, K. C. Kim, M. S. Kim, K. B. Kim, "A lithium iron phosphate/nitrogen-doped reduced graphene oxide nano composite as a cathode material for high power lithium ion batteries", J. Mater. Chem. A, **2** (2014) 9594-9599.

9 J. Zheng, L. Ni, Y. Lu, C. Qin, P. Liu, T. Wu, Y. Tang, Y. Chen, "Synthesis and characterization of $LiFePO_4$ electrode materials coated by graphene", Appl. Surf. Sci., **305** (2014) 427–432.

10 S. Wang, H. Yang, L. Feng, S. Sun, J. Guo, Y. Yang, H. Wei, "A simple and

inexpensive synthesis route for $LiFePO_4$/C nanoparticles by co-precipitation", J. Power Sources **233** (2013) 43-46.

11 G. Meligrana, C. Gerbaldi, ,A.Tuel, S. Bodoardo, N. Penazzi, "Hydrothermal synthesis of high surface $LiFePO_4$ powders as cathode for Li-ion cells", J. Power Sources **160** (2006) 516–522.

12 J. K. Kim, J. W. Choi, G. S. Chauhan, J. H. Ahn, G. C. Hwang, J. B. Choi, H. J. Ahn, "Enhancement of electrochemical performance of lithium iron phosphate by controlled sol–gel synthesis", Electrochim. Acta, **53** (2008) 8258–8264

13 M. Vujkovi, I. Stojkovi, N. Canin, S. Mentus, "Gel-combustion synthesis of $LiFePO_4$/C composite with improved capacity retention in aerated aqueous electrolyte solution", Electrochim. Acta, **92** (2013) 248– 256.

14 P. K. Patro, A. R. Kulkarni, C. S. Harendranath, "combustion synthesis of $Sr_{0.5}Ba_{0.5}Nb_2O_6$ and effect of fuel on its microstructure and its dielectric properties", Mater. Res. Bull., **38** (2003) 249-259.

15 L. D. Jadhav, S. P. Patil, A. U. Chavan, A. P. Jamale, V. R. Puri, "Solution combustion synthesis of Cu nanoparticles: a role of oxidant-to-fuel ratio", Micro Nano Lett., **6** (2011) 812 – 815.

16 G. Ramesh, R. V. Mangalaraja, S. Ananthakumar, P. Manohar, "Influence of fuel in the microwave assisted combustion synthesis of nano α-alumina powder", International Journal of Physical Sciences, **8 (34)** (2013) 1729-1737.

17 I. Ganesh, B. Srinivas, R. Johnson, B. P. Saha, Y. R. Mahajan Effect of fuel type on morphology and reactivity of combustion synthesised $MgAl_2O_4$ powders, Br. Ceram. Trans., **101:6** (2002) 247-254.

18 N. Kalaiselvi, A. Manthiram, "One-pot, glycine-assisted combustion synthesis and characterization of nano porous $LiFePO_4$/C composite cathodes for lithium-ion batteries", J.Power Sources, **195** (2010) 2894–2899.

19 B. Zhao, X. Yu, R. Cai, R. Ran, H. Wang, Z. Shao, "Solution combustion synthesis of high rate performance carbon-coated lithium iron phosphate from inexpensive iron (III) raw material", J. Mater. Chem., **22** (2012) 2900-2907.

20 S. J. Rajoba, L. D. Jadhav, R. S. Kalubarme, P. S. Patil, S. Varma, B. N. Wani, "Electrochemical performance of $LiFePO_4$/GO composite for Li-ion batteries", Ceram. Int., **44** (2018) 6886–6893.

21 A. B. Salunkhe, V. M. Khot, M. R. Phadatare, S. H. Pawar, "Combustion synthesis

of cobalt ferrite nanoparticles—Influence of fuel to oxidizer ratio", J. Alloys Compd., **514** (2012) 91– 96.

22 S. J. Rajoba, L. D. Jadhav, P. S. Patil, D. K. Tyagi, S. Varma, B. N. Wani, "Enhancement of Electrical Conductivity of $LiFePO_4$ by Controlled Solution Combustion Synthesis", J. Electron. Mater., **46** (2017) 1683-1691.

23 S. J. Rajoba, S. D. Sartale, L. D. Jadhav, "Investigating functional groups in GO and r-GO through spectroscopic tools and effect on optical properties", **175** (2018) 312-318.

24 S. V. Chavan, A.K. Tyagi, "Preparation and characterization of $Sr_{0.09}Ce_{0.91}O_{1.91}$, $SrCeO_3$, and Sr_2CeO_4 by glycine–nitrate combustion: Crucial role of oxidant-to-fuel ratio", J. Mater. Res., **19** (2004) 3181-3188.

25 K. Tahmasebi, M.H. Paydar, "The effect of starch addition on solution combustion synthesis of Al_2O_3–ZrO_2 nanocomposite powder using urea as fuel", Mater. Chem. Phys., **109** (2008) 156–163

26 Y. Bai, Y. Yin, J. Yang, C. Qing, W. Zhang, "Raman study of pure, C coated and Co doped $LiFePO_4$: thermal effect and phase stability upon laser heating", J. Raman Spectrosc., **42** (2011) 831-838.

27 J. Yang, J. Wang, X. Li, D. Wang, J. Liu, G. Liang, M. Gauthier, Y. Li, D. Geng, R. Li, X. Sun, "Hierarchically porous $LiFePO_4$/nitrogen-doped carbon nanotubes composite as a cathode for lithium ion batteries", J. Mater. Chem., **22** (2012) 7537-7543.

28 F. Fathollahi, M. Javanbakht, H. Omidvar, M. Ghaemi, "Improved electrochemical properties of $LiFePO_4$/graphene cathode nano composite prepared by one-step hydrothermal method", J. Alloys Compd., **627** (2015) 146–152.

Figure caption

Fig.1: XRD patterns of (a) G-LFP and (b) U-LFP

Fig. 2: Raman spectra of (a) G-LFP and (b) U-LFP

Fig. 3: Nitrogen adsorption and de-absorption isotherms for (a) G-LFP and (b) U-LFP

Fig. 4: SEM images of (a) G-LFP and (b) U-LFP

Fig. 5: Cyclic voltammetry profiles of (a) G-LFP and (b) U-LFP at 0.1 mV/s.

Fig. 6: Charge discharge profiles of (a) G-LFP and (b) U-LFP at 0.1C

Fig. 7: XRD patterns of (a) 4LFP (b) 5LFP and (c) 7LFP

Fig. 8: SEM images of (a) 4LFP (b) 5LFP and (c) 7LFP

Fig. 9: Charge discharge profiles of (a) 4LFP (b) 5LFP and (c) 7LFP at 0.1C

Fig. 10: Rate performance of (a) 4LFP (b) 5LFP and (c) 7LFP

Fig. 11: Cyclic voltammetry profiles of (a) 5LFP/GO (b) 7LFP/GO at 0.1 mV/s.

Fig. 12: Charge discharge profiles of (a) 5LFP/GO and (b) 7LFP/GO at 0.1C

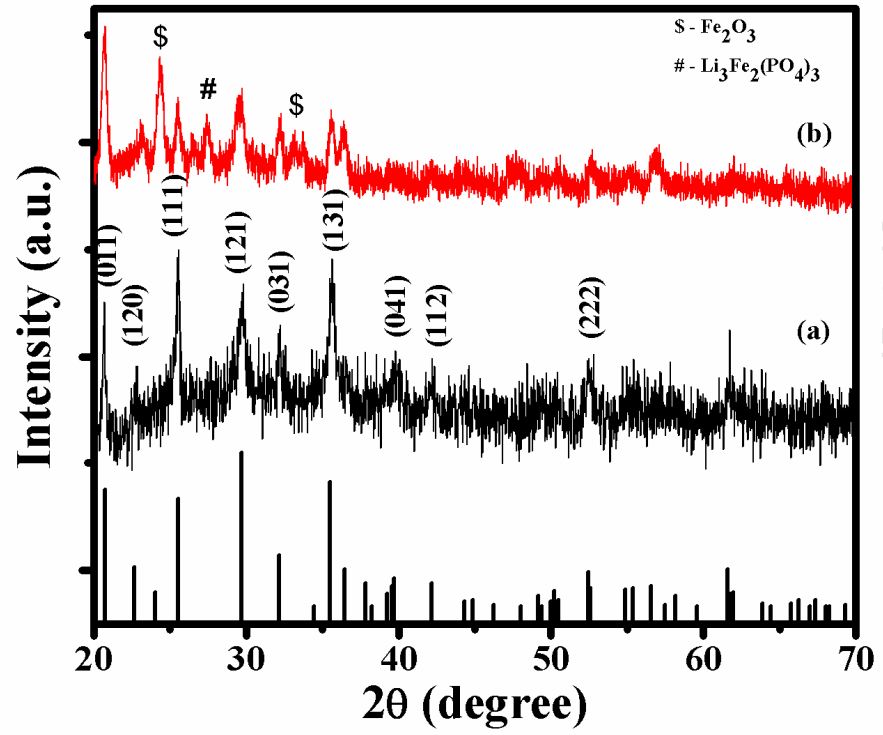
$ - Fe2O3
# - Li3Fe2(PO4)3
$
#
$
(b)
(a)
(011)
(120)
(111)
(121)
(031)
(131)
(041)
(112)
(222)
Intensity (a.u.)
20
30
40
50
60
70
2θ (degree)

Fig. 1

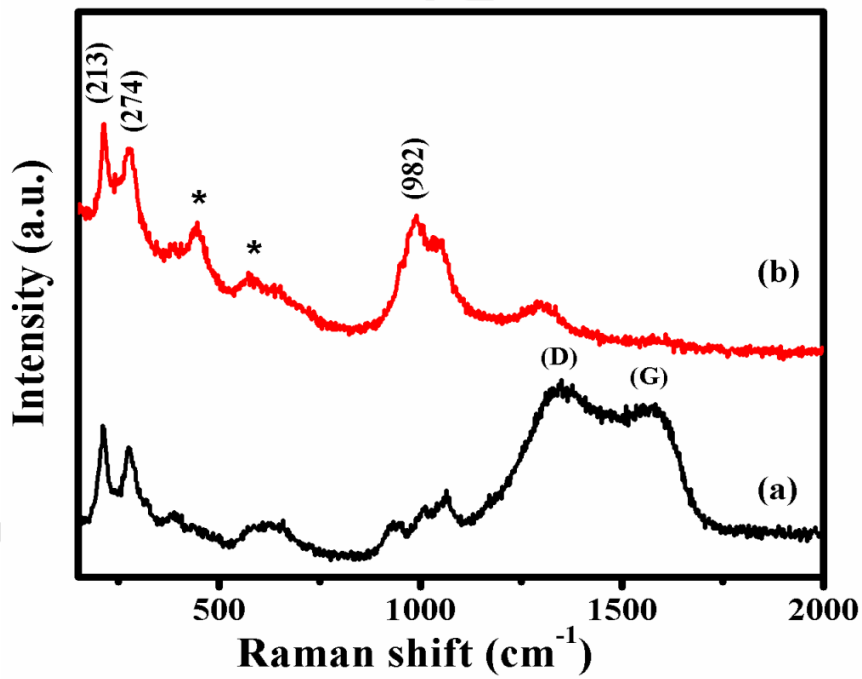
(213)
(274)
*
*
(982)
(b)
(D)
(G)
(a)
Intensity (a.u.)
500
1000
1500
2000
Raman shift (cm-1)

Fig. 2

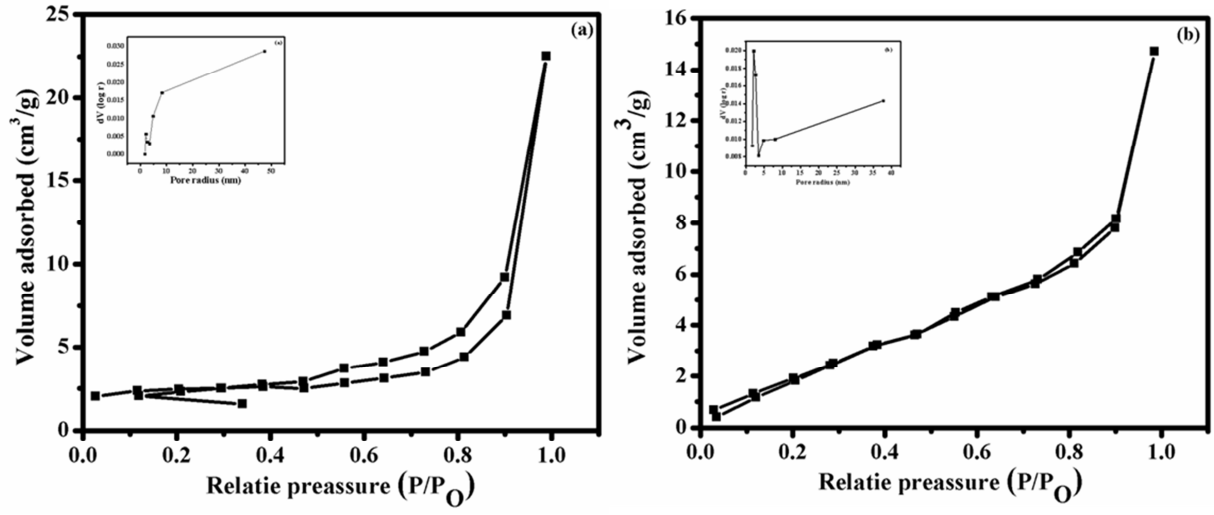
(a)
Volume adsorbed (cm3/g)
Relatie preassure (P/PO)
Pore radius (nm)
(b)
Volume adsorbed (cm3/g)
Relatie preassure (P/PO)

Fig. 3

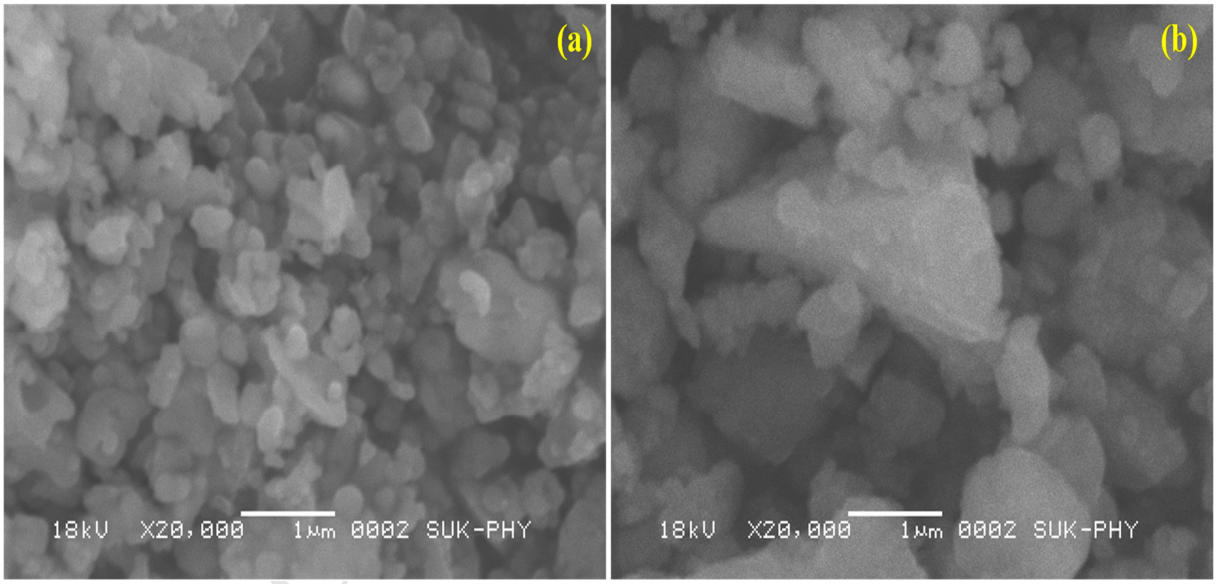
(a)
18kV X20,000 1μm 0002 SUK-PHY
(b)
18kV X20,000 1μm 0002 SUK-PHY

Fig. 4

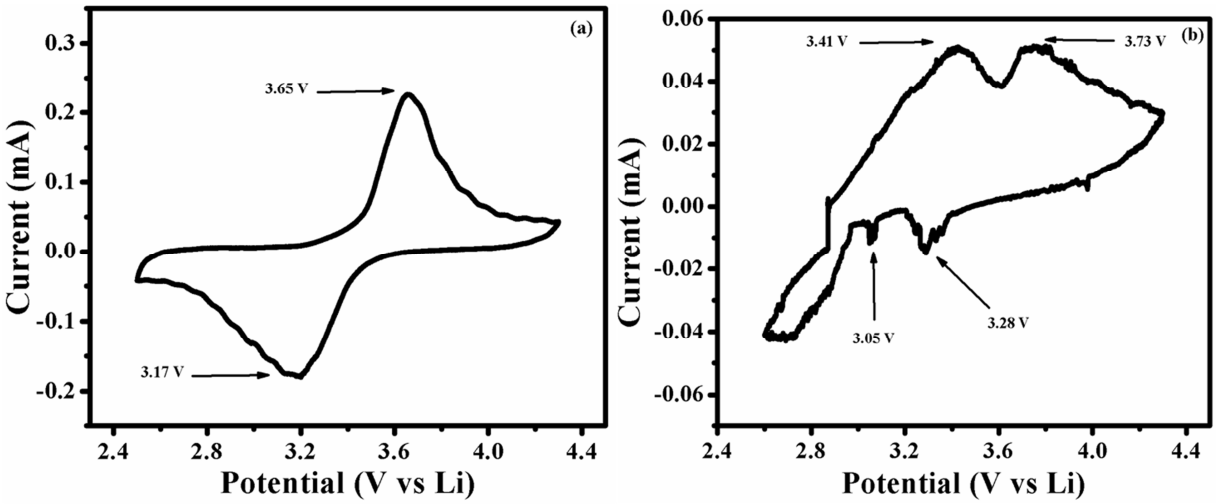
(a)
3.65 V
3.17 V
Current (mA)
Potential (V vs Li)
(b)
3.41 V
3.73 V
3.05 V
3.28 V
Current (mA)
Potential (V vs Li)

Fig. 5

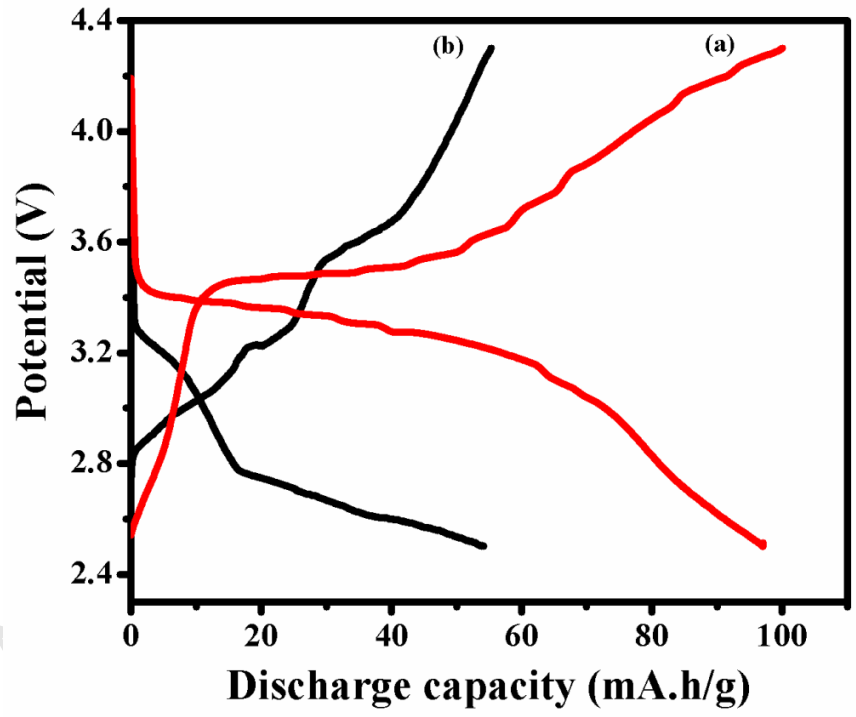
(b)
(a)
Potential (V)
Discharge capacity (mA.h/g)

Fig. 6

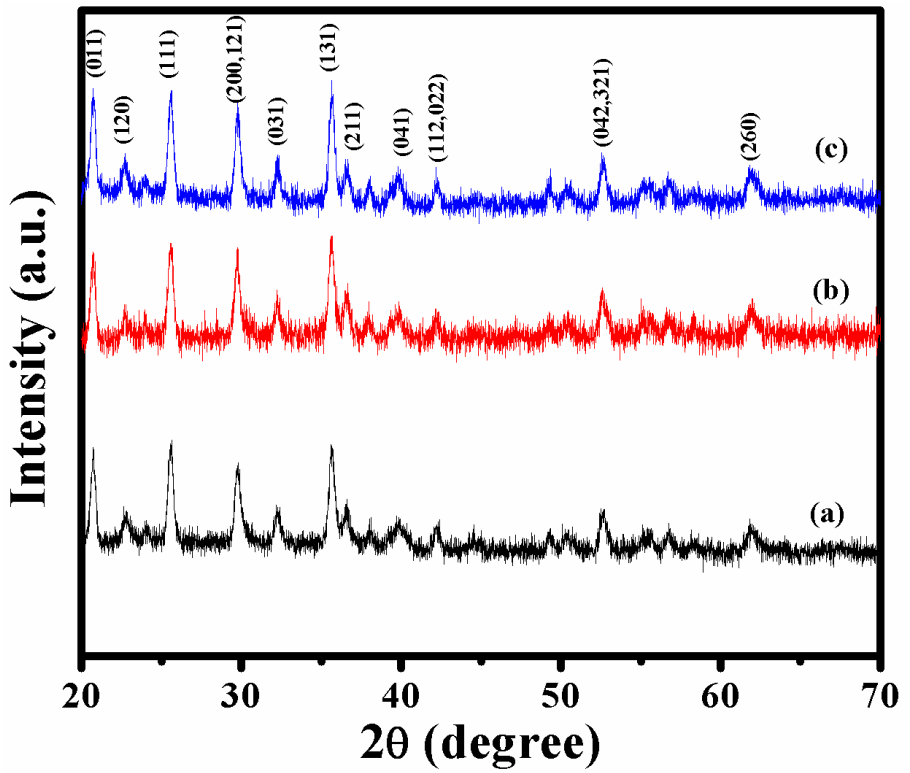
(011)
(120)
(111)
(200,121)
(031)
(131)
(211)
(041)
(112,022)
(042,321)
(260)
(c)
(b)
(a)
Intensity (a.u.)
20
30
40
50
60
70
2θ (degree)

Fig. 7

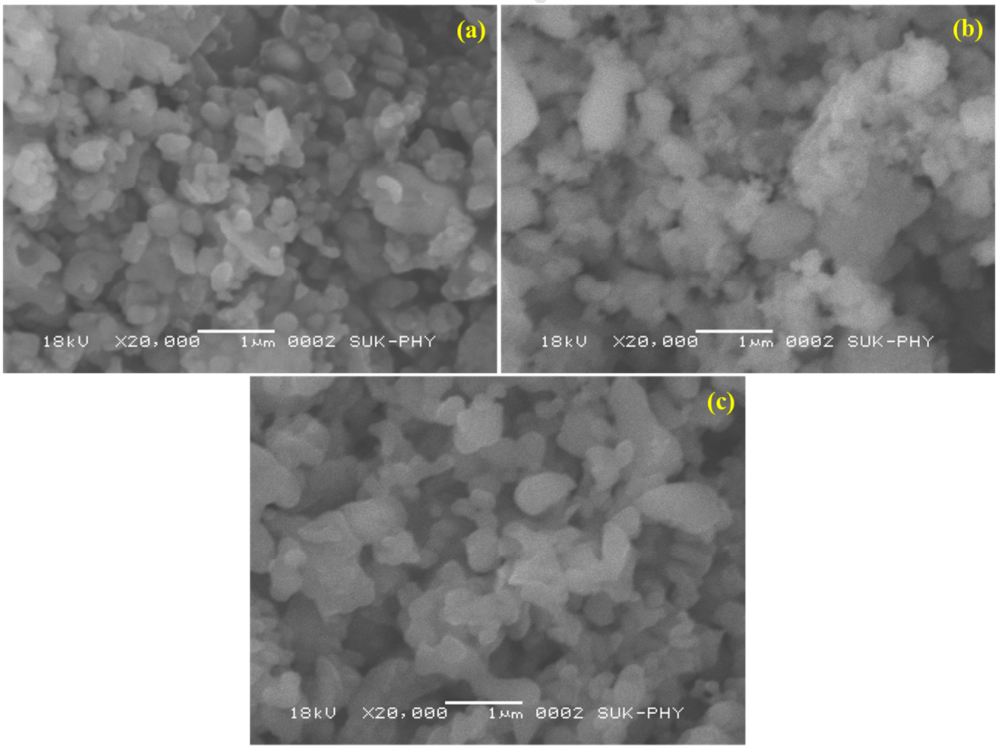
(a)
18kV X20,000 1μm 0002 SUK-PHY
(b)
18kV X20,000 1μm 0002 SUK-PHY
(c)
18kV X20,000 1μm 0002 SUK-PHY

Fig. 8

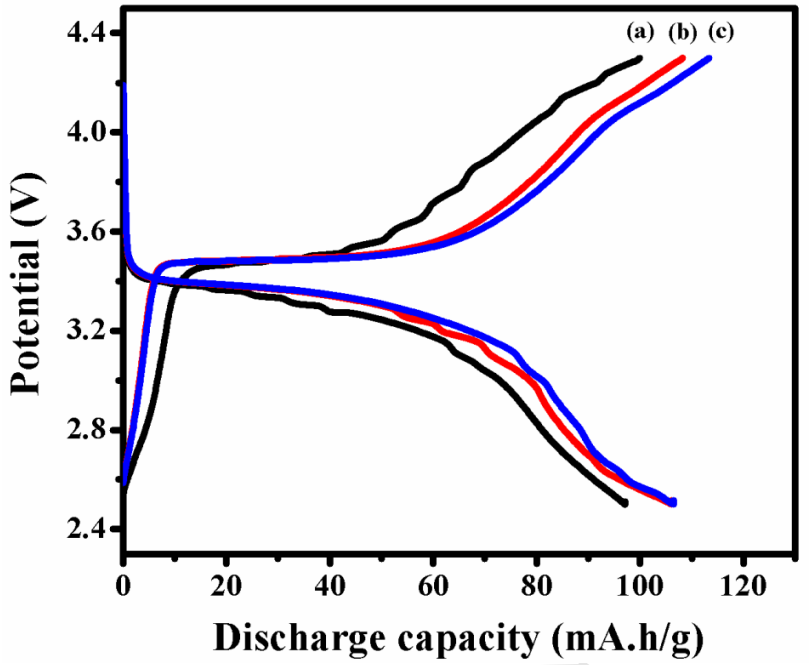
(a) (b) (c)
Potential (V)
Discharge capacity (mA.h/g)
4.4
4.0
3.6
3.2
2.8
2.4
0
20
40
60
80
100
120

Fig. 9

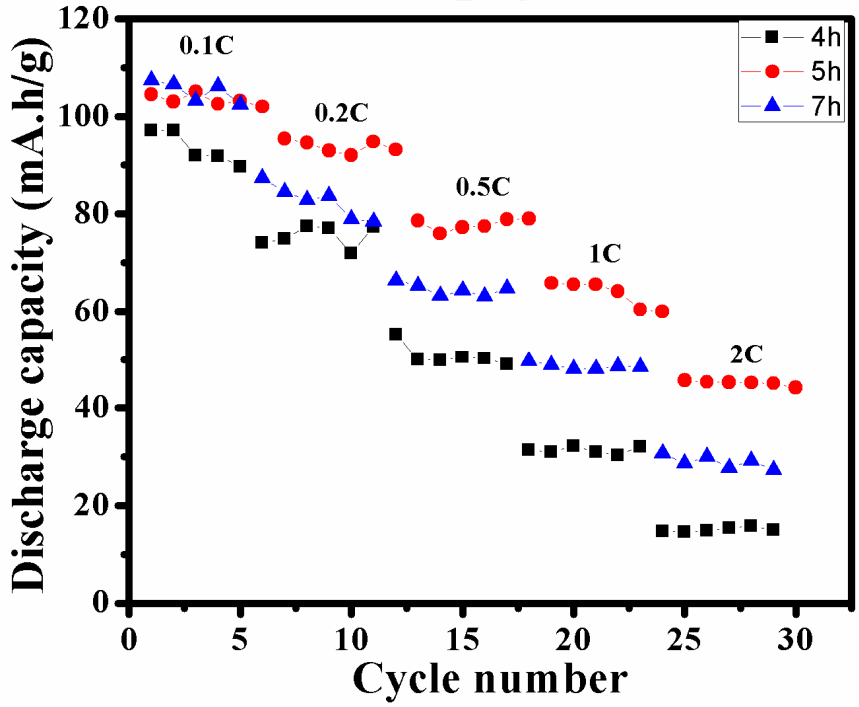
0.1C
0.2C
0.5C
1C
2C
4h
5h
7h
Discharge capacity (mA.h/g)
Cycle number
120
100
80
60
40
20
0
0
5
10
15
20
25
30

Fig. 10

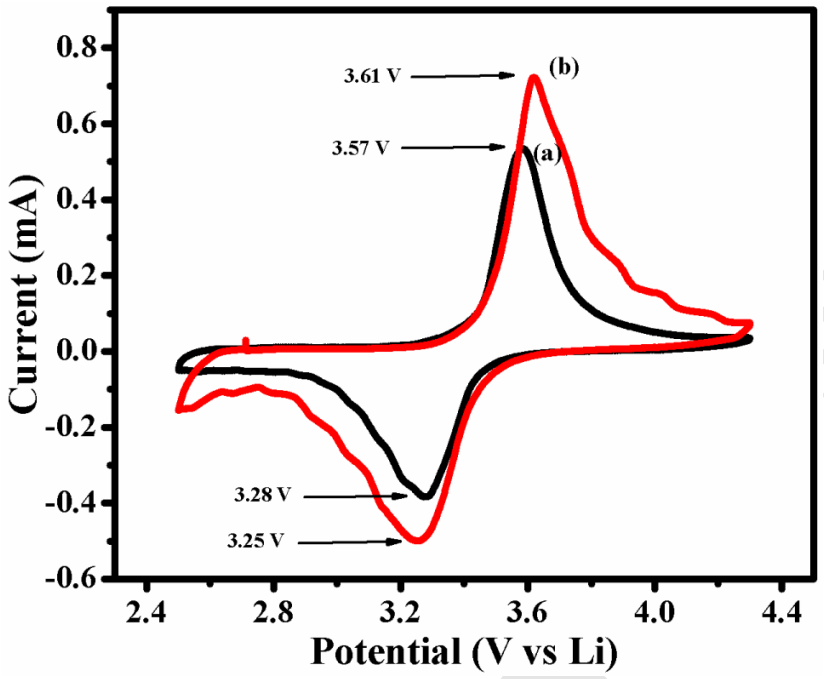
3.61 V
(b)
3.57 V
(a)
3.28 V
3.25 V
Current (mA)
Potential (V vs Li)
0.8
0.6
0.4
0.2
0.0
-0.2
-0.4
-0.6
2.4
2.8
3.2
3.6
4.0
4.4

Fig. 11

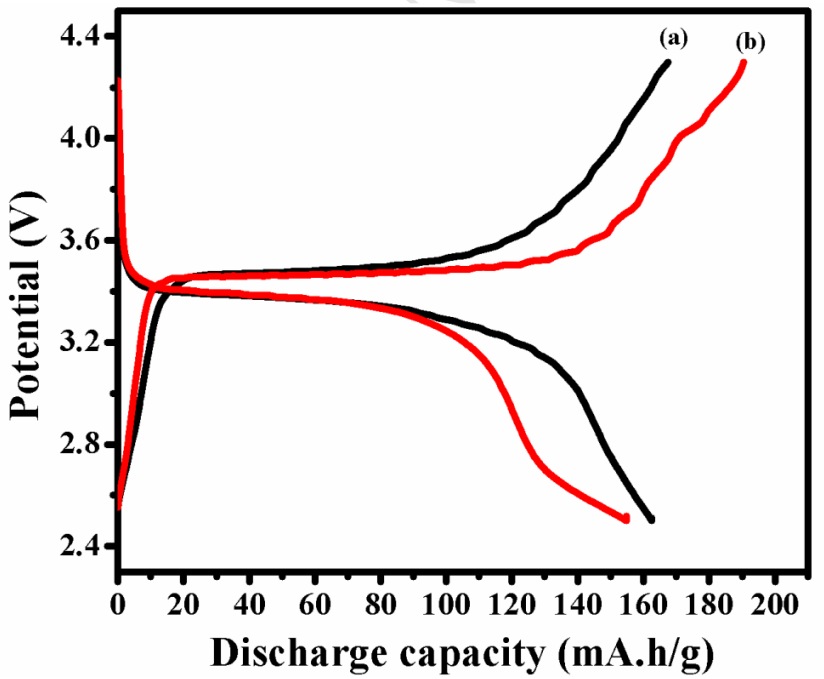
(a)
(b)
Potential (V)
Discharge capacity (mA.h/g)
4.4
4.0
3.6
3.2
2.8
2.4
0
20
40
60
80
100
120
140
160
180
200

Fig. 12

Highlights:

- ✓ Fuel controls the combustion atmosphere, temperature and particle size
- ✓ Single phase $LiFePO_4$ delivers discharge capacity of 97 mA.h/g at 0.1C
- ✓ Heat treatment affects the amount of residual carbon, grain size and porosity
- ✓ Composites 5LFP/GO and 7LFP/GO exhibit enhanced discharge capacity